Hypoxia-induced tracheal elasticity in vector beetle facilitates the loading of pinewood nematode

Xuan Tang[1,2], Jiao Zhou[1], Tuuli-Marjaana Koski[1], Shiyao Liu[1,2], Lilin Zhao[1,2]*, Jianghua Sun[3,1]*

[1]State Key Laboratory of Integrated Management of Pest Insects and Rodents, Institute of Zoology, Chinese Academy of Sciences, Beijing 1000101, China.

[2]University of Chinese Academy of Sciences, Beijing 100049, China.

[3]College of Life Science, Institute of Life Science and Green Development, Hebei University, Baoding 071002, China.

These authors contributed equally: Xuan Tang, Jiao Zhou.

*Corresponding author. Email: sunjh@hbu.edu.cn (J.S.); zhaoll@ioz.ac.cn (L.Z.)

Abstract

Many pathogens rely on their insect vectors for transmission. Such pathogens are under selection to improve vector competence for their transmission by employing various tissue or cellular responses of vectors. However, whether pathogens can actively cause hypoxia in vectors and exploit hypoxia responses to promote their vector competence is still unknown. Fast dispersal of pinewood nematode (PWN), the causal agent for the destructive pine wilt disease and subsequent infection of pine trees is characterized by the high vector competence of pine sawyer beetles (*Monochamus spp.*), and a single beetle can harbor over 200,000 PWNs in its tracheal system. Here, we demonstrate that

PWN loading activates hypoxia in tracheal system of the vector beetles. Both PWN loading and hypoxia enhanced tracheal elasticity and thickened the apical extracellular matrix (aECM) of the tracheal tubes. We observed a notable upregulation of an aECM gene *Muc91C*, encoding a resilin-like mucin protein in PWN-loaded and hypoxic tracheal tubes. RNAi knockdown of *Muc91C* reduced tracheal elasticity and aECM thickness under hypoxia conditions and thus decreasing PWN loading. Our study suggests a crucial role of hypoxia-induced developmental responses in shaping vector tolerance to the pathogen and provides clues for potential molecular targets to control pathogen dissemination.

Introduction

Insect vectors are obligatory for the dispersal of many pathogens, including several viruses and parasites deleterious to plant and animal health. Vector competence is pivotal for the successful pathogen arrival and infection of the target host, and is determined by a sophisticated set of direct interactions as pathogens enter, spread, replicate and retain within vector cells and tissues (Bartholomay and Michel, 2018; Gray et al., 2019; Lataillade et al., 2020). Therefore, pathogens have evolved to modulate various defensive responses of vectors, such as autophagy or apoptosis, as has been shown in some leaf-, planthoppers and mosquitoes, to influence vector competence (Chen et al., 2017; Huang et al., 2015; O'neill et al., 2015). Although understanding the responses that pathogens induce to manipulate vector competence is

important for developing efficient management strategies, the underlying mechanism remains largely elusive.

A pathogen of pine trees, *Bursaphelenchus xylophilus*, commonly known as pine wood nematode (PWN), is transmitted by cerambycid beetles of the genus *Monochamus* and causes pine wilt disease in millions of hectares of pine forests across Asia and Europe (Akbulut and Stamps, 2012). PWN's life cycle has two distinct developmental phases, namely the propagative stage (L_1-L_4 juveniles and reproductive adult) that propagates inside pine trees and the dispersal stage (L_{III} and L_{IV} juveniles) characterized by its close relationship with the vector beetle that transports the nematode to new host trees (Aikawa, 2008; Zhao et al., 2014). The dispersal L_{IV} enters the tracheal system of the adult beetle through the spiracles and inhabits the trachea for several days until the vector beetle has reached a new healthy host tree. The number of dispersal L_{IV} carried by an adult beetle is a critical factor influencing the damage level of the pine wilt disease in the pine host tree (Togashi, 1985). Extraordinarily, each primary vector beetle, such as *Monochamus alternatus* in Asia, can harbor on average 15,000 and up to 280,000 nematodes in its tracheal system (Fielding and Evans, 1996). In contrast to circulative pathogens that move from gut lumen to salivary glands or ovary (Eigenbrode et al., 2018; Wei et al., 2017), and to other non-circulative pathogens that typically remain in the mouthparts (Uzest et al., 2007) and foregut of their vectors (Chen et al., 2011), PWNs merely reside, and do not multiply in the tracheal systems. However, the effects of PWN on its unique resident niche (i.e., the vector tracheal

system), and the mechanism behind the vector's competence for loading of such large numbers of PWN is still poorly understood.

Hypoxia, which occurs when oxygen supply is inadequate, is common in mammal host tissues faced with infection by pathogens and induces several adaptive responses that improve host defense by maintaining the integrity of epithelial barriers and hindering the internalization process (Zeitouni et al., 2016). Recent studies suggest a modulator role of hypoxia in various biotic interactions. For example, the parasite *Trypanasoma brucei* has evolved a way to inhibit hypoxic responses to evade the host immune response in the bloodstream (Mcgettrick et al., 2016). In contrast, a mosquito gut bacterium benefits their hosts by activating hypoxic responses improving host gut growth (Coon et al., 2017; Valzania et al., 2018). As the trachea of the adult vector beetle is packed with nematodes, reduced gas transfer ability and its consequent hypoxia are conceivable.

The insect trachea, an interconnected network of air-filled epithelial tubes that exhibit optimal diameter, length and intense compression and expansion for respiration, which resembles the deflation and inflation of vertebrate lungs, supports efficient gas circulation and diffusion (Hayashi and Kondo, 2018; Westneat et al., 2003). To increase oxygen supply, the tracheal system is adapts to hypoxia by compensatory morphological and physiological changes (Harrison et al., 2018), such as tracheal terminal branching (Centanin et al., 2010) and compression of tracheal tubes (Greenlee et al., 2013). Mechanical properties of the tracheal tubes are therefore prerequisites for regulating the tracheal geometry and compression capacity and mainly depend on a

viscoelastic material surrounding tracheal lumen, called apical extracellular matrix (aECM) (Dong et al., 2014; Hayashi and Kondo, 2018; Zuo et al., 2013). In *Drosophila melanogaster*, aECMs components including serpentine, verm and dumpy affect aECM elasticity, and have been reported to mediate the tubular diameter or length, possibly by restricting apical membrane growth (Luschnig et al., 2006; Wilkin et al., 2000). A study with the American cockroach (*Periplaneta americana*) suggested that chitin structures in aECM layer are responsible for the mechanical features that enable tracheal compression and volume change during respiration (Webster et al., 2011). In addition, hypoxia has been shown to correlate with overall aECM composition and organization of blood vessels and respiratory networks (Jang et al., 2021; Kusuma et al., 2012), implying a possible link between hypoxia and the molecular components contributing to mechanical properties of the tracheal tubes. Taken together, we hypothesize that hypoxia may be involved in the retention of PWN in vector beetle's tracheal system through the PWN exploiting mechanical properties of the vector beetle's trachea to maintain a high vector capacity in a hypoxia-regulated manner.

Here, we revealed that the number of the nematodes in the trachea is negatively correlated with the oxygen level in the tracheal system of its vector beetle, leading to hypoxia. Both PWN loading and hypoxia enhanced the elasticity of tracheal tubes and increased the thickness of aECMs in tracheal epithelia. Based on transcriptome analysis of trachea with and without PWN, we identified aECM-related genes in the beetles and found a candidate aECM component, a resilin-like mucin protein Muc91C, the expression of which was substantially upregulated after PWN loading and hypoxic

treatment. *Muc91C* knockdown reduced elasticity of the tracheal tubes and aECMs thickness under hypoxic condition, indicating that *Muc91C* help regulate the aECM-related mechanical traits of the tracheal tubes. Importantly, RNAi of *Muc91C* in adult beetles significantly reduced PWN loading in trachea. These results demonstrate crucial roles of tracheal hypoxia and aECM-related tubular elasticity in improving vector competence for PWN transmission.

Results

PWN loading decreased oxygen levels in the tracheal system of vector beetle

To determine whether PWN loading reduces oxygen levels and caused hypoxia in trachea of vector beetles, we first measured the concentration of oxygen inside major thoracic tracheal tubes using an oxygen microsensor (**Figure 1A**). Radial oxygen profiles revealed a slight drop of oxygen pressure from 21kPa to 18.9kPa, respectively, when comparing pressure outside (i.e., in the ambient air) and inside the tracheal tubes of beetles without PWN. In contrast, there was a dramatic drop of oxygen pressure from 21kPa outside of tubes to 3.8kPa inside tubes when trachea was loaded with PWN (**Figure 1B**). Thus, our results showed that PWN loading induce oxygen shortage in trachea.

We further established the correlation between oxygen level and total number of nematodes in the trachea by measuring the oxygen concentration in the atrium cavity of the first and largest abdominal spiracles and calculating the number of nematodes in the beetle (**Figure 1A**). The partial pressure of oxygen was negatively correlated with

127 the total number of nematodes in tracheal tissue per 0.3g beetle (**Figure 1C**). The curve
128 fit to this data revealed that when the total number of nematodes reached 10,000, partial
129 pressure of oxygen in the cavity of tracheal spiracle dropped to 10 kPa (half of the
130 corresponding value in the surrounding air (usually 21 kPa), creating a mild hypoxia at
131 approximately PO_2 of 5-15 kPa. In addition, when the number of nematodes increased
132 to 44,828, the oxygen pressure dropped dramatically to 4 kPa (**Figure 1C**), which is the
133 threshold between mild and severe functional hypoxia in *Drosophila* (Harrison et al.,
134 2018). Oxygen levels in the cavity of the atrium were further compared among three
135 levels of PWN loading, differing in total number of nematodes in the trachea. The
136 tracheal systems of beetles without PWN (Null) or with light PWN loading (< 10,000)
137 had an oxygen pressure equal to that of the environment. By contrast, substantial
138 decline to approximately 4kPa of oxygen were detected in the tracheal spiracle with
139 heavy PWN loading (> 10,000). These results indicated PWN loading caused hypoxia
140 or anoxia in the trachea of vector beetles.

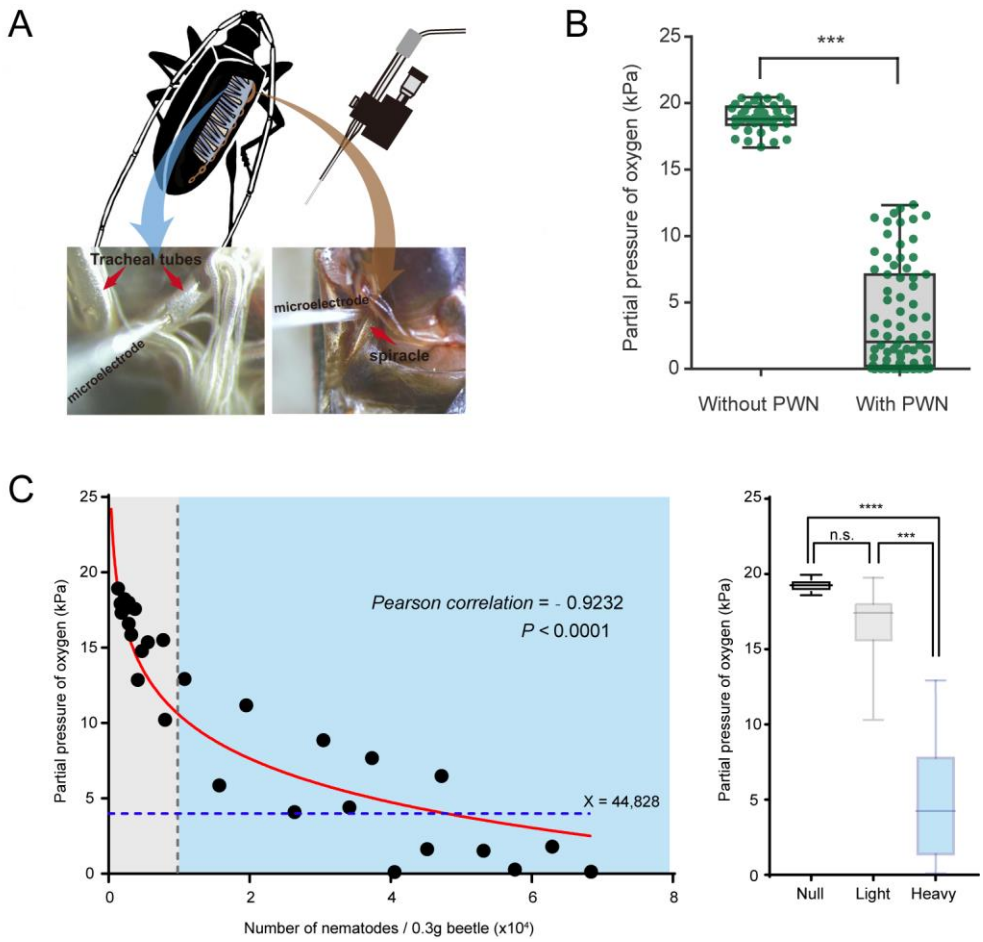

Figure 1. Negative correlation between oxygen level and PWN loading in tracheal system of *M. alternatus*. (**A**) Schematic representation of experimental setup used for microelectrode (top right) measurements inside a major trachea tube of the thorax (bottom left) and the atrium cavity of the largest spiracle (bottom right). (**B**) Partial oxygen pressure in the tracheal tubes of vector beetles with and without PWN (N = 38 and 76 tracheal tubes in 5 adults, respectively). ***$P < 0.0001$ (Mann–Whitney U test). The internal lines are medians, edges of the boxes are interquartile ranges and whiskers are minimum and maximum ranges. (**C**) The relationship between oxygen partial pressure in atrium of vector beetle (N = 5, 17 and 14 adults for null, light and heavy PWN loading) and the number of nematodes. Left panel: Fitted curve is drawn in red

line. The gray line, which shows 10,000 PWN, divides beetle samples into light or heavy PWN loading. The blue line shows the estimated loading number of nematodes when partial pressure drops to 4kPa. Right panel: Partial pressure of oxygen in atrium of beetles in three different degrees of PWN loading. ***$P = 0.0001$, ****$P < 0.0001$ (Kruskal–Wallis nonparametric test, Dunn's multiple comparison test). The internal lines are medians, edges of the boxes are interquartile ranges and whiskers are minimum and maximum ranges.

Nematode-induced hypoxia enhanced tracheal elasticity and thickened its apical extracellular matrix

Compared to those free of PWN, the trachea of vector beetles bearing PWN tended to be rubberlike (**Figure 2-figure supplement 1A**). The total number of the nematodes in the trachea correlated positively with the tracheal rubberization degree (**Figure 2-figure supplement 1B**). Trachea with the highest rubberization degree released five times more nematodes (reaching approximately 16,000 nematodes on average) compared to trachea with moderate or low rubberization. Preliminary observations further showed that the trachea tubes harboring PWN tended to be longer and narrower before breakage under external force (**Figure 2-figure supplement 2 and Video 1 and Video 2**). This relationship indicated that PWN loading influenced the mechanical properties of the vector's trachea.

The elasticity of trachea tubes was further quantified by comparing Young's modulus values of tracheal tubes among the three levels of PWN loading (null, light and heavy)

173 mentioned above. Corresponding to their higher oxygen level, Young's modulus values
174 of trachea tubes without PWN and with light PWN loading were almost two times
175 higher than the values in hypoxic trachea tubes with heavy PWN loading (**Figure 2A**).
176 Given the negative correlation between elasticity and Young's modulus values, this
177 result suggested that heavy PWN loading enhanced tracheal elasticity. To confirm the
178 influence of hypoxia on tracheal elasticity, we subjected beetles free of PWN to 1% O_2
179 for 6 h, 12 h and 24 h. Compared with that of tracheal tubes exposed to normoxia and
180 hypoxia conditions for 6h, the Young's modulus values under hypoxic treatments for
181 12h and 24 h decreased by nearly a half (**Figure 2A**). These results clearly demonstrated
182 that heavy PWN loading and its induced hypoxia enhanced tracheal elasticity.

183 Due to the correlation between mechanical properties and apical extracellular matrix
184 (aECM), we further investigated the tracheal structure with null and heavy PWN
185 loading using transmission electron microscopy. Micrographs revealed that the secreted
186 protein layer of tracheal aECM was significantly thickened by heavy PWN loading
187 (**Figure 2B and C**). However, the heavy PWN loading had no effect on the morphology
188 of the chitin layer of aECM. To examine the effect of hypoxia on tracheal aECM, we
189 treated beetles free of PWN with 1% O_2 for 6h, 12h and 24h. Electron micrographs
190 showed that the secreted protein layer of tracheal aECM under hypoxia for 12h and 24h
191 was thicker than those under normoxia and hypoxia for 6h (**Figure 2C**). Therefore, our
192 results indicated that PWN-induced hypoxia promoted the secretion of protein layers in
193 aECM in trachea. Taken together, these results suggest that the increased secretion of
194 protein layer of aECM was involved in enhanced tracheal elasticity by PWN-induced

hypoxia.

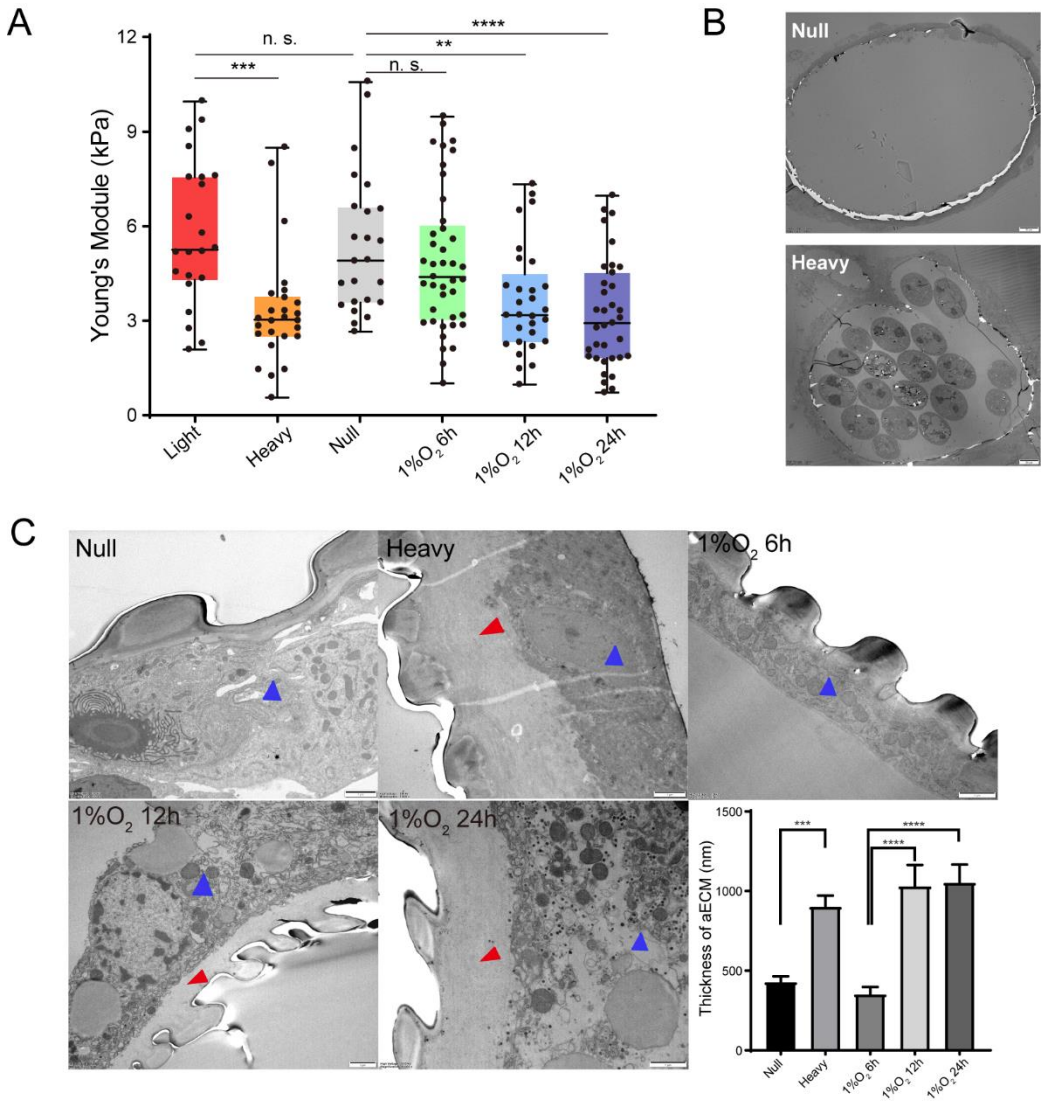

Figure 2. Effects of PWN loading and hypoxia on mechanical properties and apical extracellular matrix (aECM) of the trachea tubes of *M. alternatus*. (**A**) Calculated Young's modulus in different experimental groups according to values in tensile test in the longitudinal direction on the longest tubes linking two homolateral spiracles. Groups represent tubes from beetles without PWN (Null), light (< 10,000 nematodes), heavy (> 10,000 nematodes) PWN loading, and treated with 1% O_2 for 6h, 12h and 24h, respectively (N = 22 - 41 tracheal tubes for each treatment). $^{**}P < 0.01$, $^{***}P < 0.001$ and $^{****}P < 0.0001$ (Kruskal–Wallis nonparametric test, Dunn's multiple comparison

205 test). Internal lines are medians, edges of the boxes are interquartile ranges and whiskers
206 are minimum and maximum ranges. (**B** and **C**) Transmission electron micrographs
207 (TEMs) for axial views of the longest tracheal tubes. (**B**) Representative images were
208 shown for global view of tracheal tubes without (Null) and with heavy PWN loading.
209 Bars, 20μm. Experiments were performed at least three times. (**C**) Electron microscopy
210 images showed the thickened tracheal aECM (red arrow) between the chitin layer
211 (taenidial ridges) and the body of tracheal cell (blue arrow) after different treatments
212 (without PWN, i.e. Null, heavy PWN, and 1% O_2 for 6h, 12h and 24h, respectively).
213 Bars, 1μm. The right bottom panel shows the statistical data of the thickness of aECM
214 corresponding to TEMs. Data were measured in 6 tracheal tubes of 3 adults for each
215 treatment. ***$P < 0.001$ and ****$P < 0.0001$ (Kruskal–Wallis nonparametric test,
216 Dunn's multiple comparison test). Data are represented as mean ± SEM.

217 **PWN loading caused significant upregulation of *Muc91C* in trachea**

218 To confirm the role of proteins to the enhanced tracheal elasticity, we compared the
219 tracheal transcriptomes between PWN free and heavily PWN loaded beetles and
220 discovered 916 differentially expressed genes (DEGs). Out of these, 251 DEGs were
221 identified as aECM-related genes (**Figure 3A**). Overall, the altered transcript profiles
222 suggested dramatic epithelium reorganization in tracheal tubes of vector beetles after
223 PWN loading. We then chose 45 genes related to mechanical properties to further
224 scrutinize for their expression (**Figure 3B**). We examined chitinases, chitin synthases
225 and chitin deacetylases, which are involved in chitin catabolic processes, biosynthetic

226 processes, and arrangement, respectively (Dong and Hayashi, 2015). The up or down
227 regulated pattern in the expression of these transcripts suggested a chitin metabolic
228 equilibrium, which was consistent with the unchanged chitin layer among beetles with
229 heavy PWN loading shown in TEMs (**Figure 2C**). Our gene list also included those
230 genes functioning as aECM regulators. For example, Metalloproteinases are
231 proteinases that cleave proteins in the extracellular matrix (Glasheen et al., 2010).
232 Cadherins, integrins, lachesin and dumpy are transmembrane proteins participating in
233 signal transduction between aECM and tracheal cells (Llimargas et al., 2004; Öztürk-
234 Çolak et al., 2016; Wilkin et al., 2000). The changed expression of these transcripts
235 after heavy PWN loading indicated altered regulatory cascades of aECM. We finally
236 investigated the expression of the non-chitin structural components including mucins,
237 collagens and laminin. Negatively regulated transcripts of collagens in heavy loading
238 PWN samples and the location of laminin in basal lamina of tracheal cells (Dai et al.,
239 2018) suggest they were not responsible for thickening the aECM layer in our
240 observations (**Figure 2C**). Therefore, the genes encoding for the mucin family, a group
241 of large glycosylated macromolecules, are possible candidate genes contributing to the
242 elasticity of trachea in our study, because their location and upregulation directly
243 corresponded to the observed thickened non-chitin layer in aECMs visible in electron
244 microscopy (**Figure 2C**). Among the three mucin genes, *Muc91C* had the highest
245 increase in expression after PWN loading, increasing more than seven folds (log2FC =
246 2.43), higher than the other two genes (**Figure 3A**).

247 Further analysis of gene structure revealed that *Muc91C* encoded a resilin-like

248 protein (Andersen, 2010), dominated by two long regions containing a series of short
249 repeat motifs (**Figure 4**). Seventeen A repeats, with the consensus sequence
250 PSSSYGAPA(S) were located in the N-terminal region. Additionally, eleven B repeats,
251 with the consensus sequence GGYSSGGN, were located in the C-terminal region. As
252 the only identified MaMuc91C homolog in insects, DmMuc91C was identified
253 previously as a pro-resilin protein. In addition, a BLASTX search of MaMuc91C
254 against Flybase revealed its similarity not only to DmMuc91C (CG7709-PB) but also
255 to functional DmPro-resilin (CG15920-PA). Using DmPro-resilin and resilin-like
256 DmMuc91C as query sequences in turn, we further characterized 17 resilin-related
257 genes in the tracheal transcriptome of the PWN vector beetle and in the genomes of
258 other insects. Phylogenetic analysis revealed that MaMuc91C and six proteins from
259 other insects were assigned to clade I, which share repeat A motif with a consensus
260 sequence of PS(Q)SSYGAP(A)S. Importantly, sequence in clade I shared two features
261 with pro-resilin proteins. First, the glycine and proline residues, indicating its long-
262 range elasticity. Second, a tyrosine residue, which presumably facilitates the formation
263 of dityrosine crosslinks after secretion from the epidermal cells. However, clade I
264 lacked the chitin binding R&R consensus sequence, a defining feature of true pro-resilin.
265 Thus, this protein was classified as a resilin-like protein. Based on the PTS domain and
266 O-glycosylation sites (Zhao et al., 2020), we found that all the proteins in clade I
267 (**Figure 4**) belonged to the mucin family and may be homologs of Muc91C, given their
268 similarity with DmMuc91C. The other six resilin-related proteins were clustered into
269 clade II, in which repeat A motifs were highly variable and all sequences contained the

270 chitin binding R&R consensus. In addition, phylogenetic analysis based on *M.*
271 *alternatus.* and other insect species' mucin sequences showed that Muc91C proteins
272 were clustered into a separate lineage (**Figure 4-figure supplement 1**). We therefore
273 conclude that *MaMuc91C* encodes a resilin-like protein with potential long-range
274 elasticity.

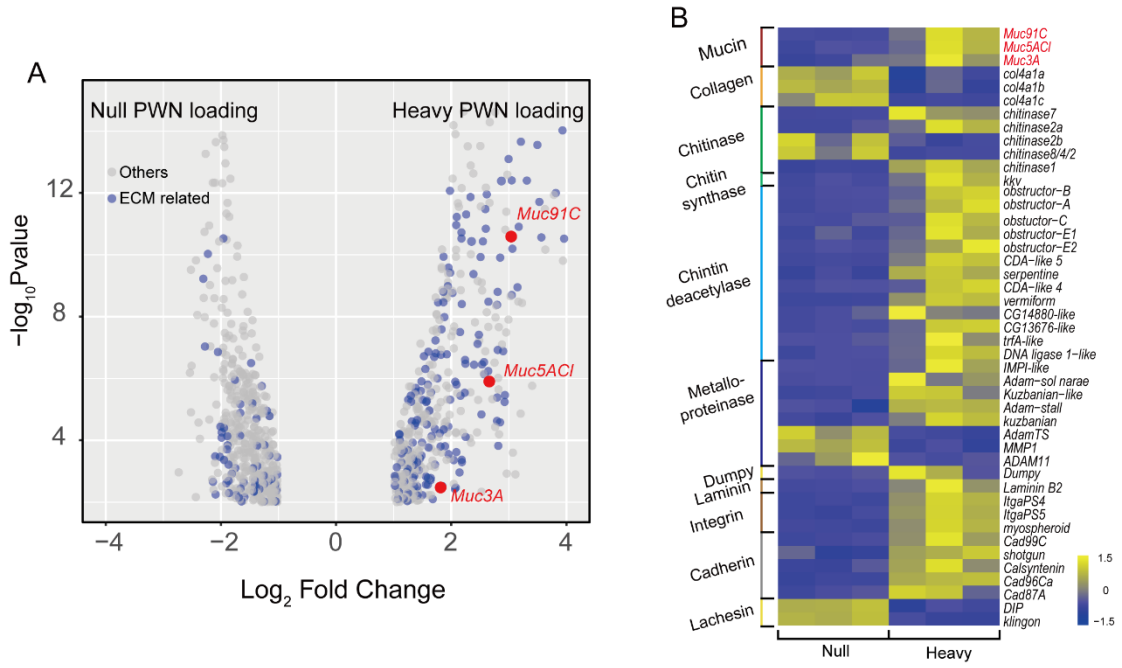

275

276 **Figure 3. Transcriptome analysis showed changed expression pattern of aECMs-**
277 **related genes in trachea treat with PWN.** (**A**) Volcano plot of RNA-seq data from
278 trachea of beetles with and without PWN. Grey dots indicate all DEGs, and blue dots
279 indicate aECM-related DEGs. The red dots indicate the three mucins. (**B**) Heat map of
280 differential expressed genes related to mechanical property of tracheal tubes of beetles
281 with and without PWN. The red font indicates the three mucins.

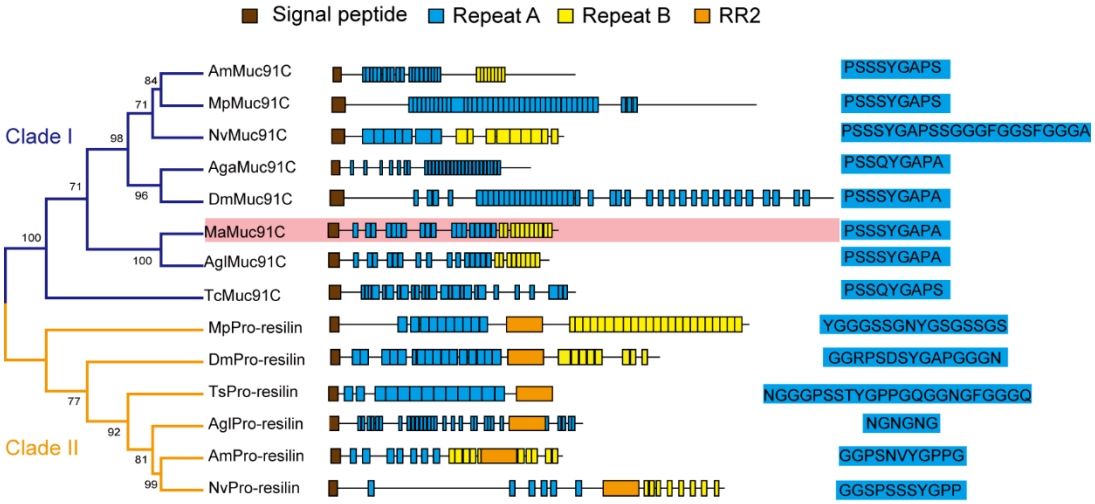

Figure 4. Phylogenetic relationship among resilin-related proteins in insects. The phylogenetic analysis was performed using the full-length amino acid sequences of representative resilin-related proteins. The blue and yellow branches represent Muc91C (Clade I) and Pro-resilin (Clade II), respectively. The domain architectures are listed at the middle panel. Brown boxes indicate signal peptide. Blue boxes indicate repeats A. Yellow boxes indicate repeats B. Orange boxes indicate RR2. The consensus sequences of repeats A are listed at the right panel. MaMuc91C is highlighted in pink.

Muc91C contributes to hypoxia-enhanced trachea elasticity and promote PWN loading

We independently validated our RNA-seq results by repeating the experiment using new individuals and quantifying expression using reverse-transcription qPCR (RT-qPCR) for the genes that belong to the mucin family. In contrast to the other two mucin genes, the abundance of *Muc91C* transcripts positively correlated with the level of PWN loading in trachea (**Figure 5A**). Compared to that of trachea without PWN, the expression level of the *Muc91C* gene increased five-fold in trachea with heavy PWN

298 loading. To test the effect of hypoxia on *Muc91C*, *Muc5ACl* and *Muc3A*, gene
299 expression levels were measured after exposure of beetles under 1% O2 for 6h, 12h and
300 24h. Hypoxia treatment of 12h caused significant upregulation of Muc91C in trachea
301 (**Figure 5B**). Therefore, we conclude heavy PWN loading in beetles' trachea stimulates
302 the expression of *Muc91C* via inducing hypoxia.

303 We further verified the key role of *Muc91C* in determining the thickness of aECM
304 and its related elasticity under hypoxia condition. Firstly, we used TEM to observe the
305 substructure of tracheal tubes treated with 1% O_2 for 12h, after performing gene
306 knockdown of *Muc91C* in adult beetles. RNAi knockdown of *Muc91C* resulted in a
307 77.5% decrease in *Muc91C* mRNA levels (**Figure 5-figure supplement 1**). Compared
308 to ds*GFP*-injected beetles, the thickness of aECM layers in tracheal tubes were
309 substantially reduced in ds*Muc91C*-injected beetles (**Figure 5C**). Next, we measured
310 Young's modulus values of trachea tubes treated with 1% O_2 for 12h after dsRNA
311 injection. Compared to the ds*GFP* control, the Young's modulus values of tracheal
312 tubes were significantly increased in the ds*Muc91C* samples, indicating their decreased
313 elasticity after *Muc91C* knockdown (**Figure 5D**). Therefore, the enhanced tracheal
314 elasticity induced by hypoxia relies on the expression of *Muc91C*.

315 To further confirm the role of *Muc91C*-induced elasticity in PWN loading, we carried
316 out *Muc91C* knockdown in adult beetles and subsequently inoculated beetles with
317 PWN. Compared to beetles injected with ds*GFP*, the number of nematodes in beetles
318 injected with ds*Muc91C* was reduced by 50%, and the total number of nematodes in
319 these beetles' trachea reaching less than 10,000 (**Figure 5E**). Collectively, *Muc91C* was

320 essential to promote heavy PWN loading by promoting tracheal elasticity during

321 hypoxia.

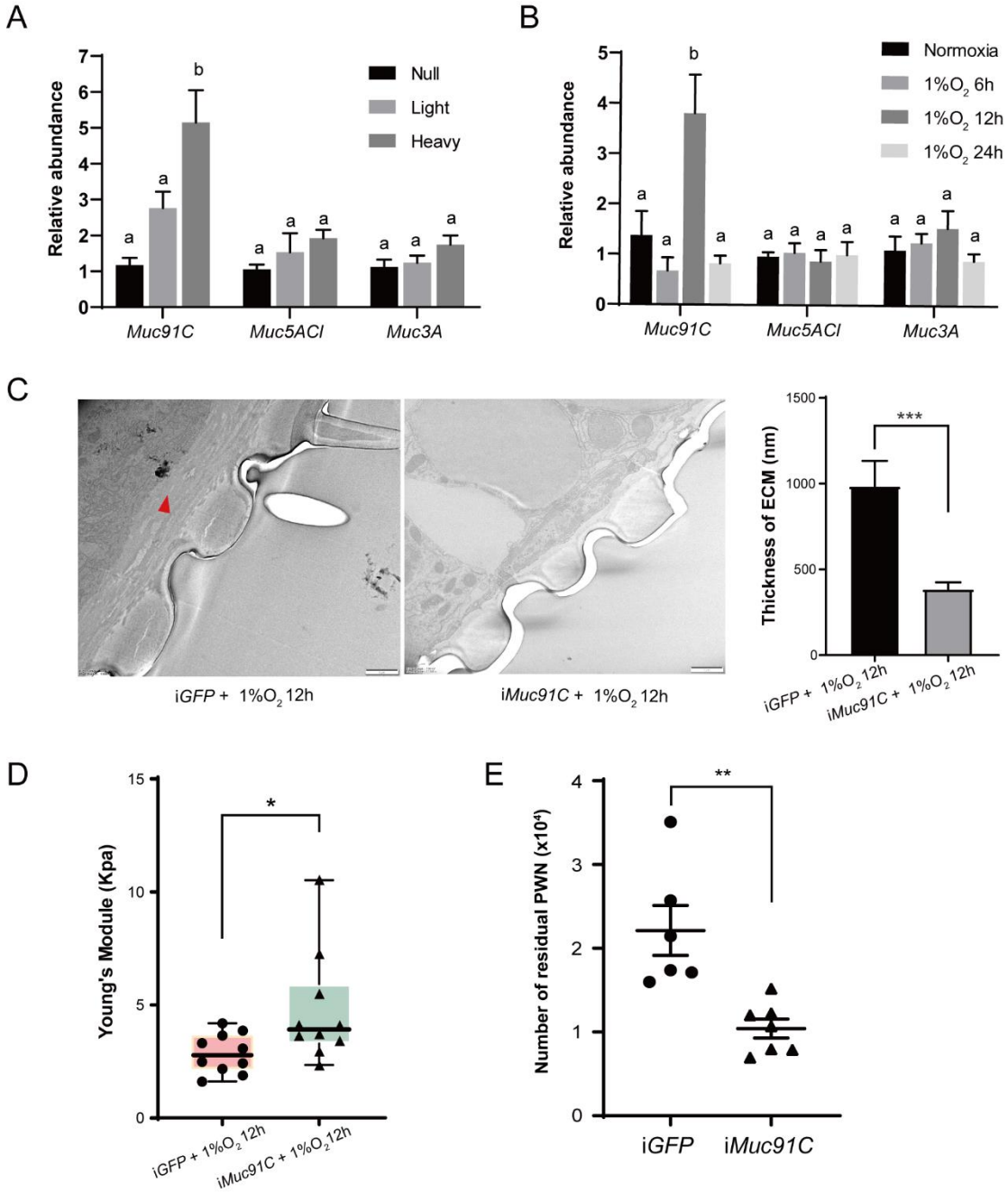

322

323 **Figure 5. The role of *Muc91C* in tracheal elasticity and PWN loading.** (**A**) Relative

324 RNA abundance of three genes belonging to mucin family in trachea of beetles with

325 null, light (< 10,000 nematodes) or heavy (> 10,000 nematodes) PWN loading. Data

326 are represented as mean ± SEM. Columns labeled with different letters indicate

statistically significant differences in mean relative abundance (N = 7-8 for each gene, one-way ANOVA with Tukey's multiple comparisons, P = 0.0003, 0.1992, 0.1353 for *Muc91C*, *Muc5ACl* and *Muc3A*, respectively). (**B**) Relative RNA abundance of three genes belonging to mucin family in trachea of beetles under normoxia or 1% O_2 for 6h, 12h, or 24h. Data are represented as mean ± SEM. Columns labeled with different letters indicate statistically significant differences in mean relative abundance (N = 5 for each gene, one-way ANOVA with Tukey's multiple comparisons, P = 0.0009, 0.9389, 0.3662 for *Muc91C*, *Muc5ACl* and *Muc3A*, respectively). (**C**) Electron microscopy images showed the thickened tracheal aECM (red arrow) under 1% O_2 for 12h after ds*GFP* or ds*Muc91C* injection. Bars, 1μm. The right panel shows the statistical data of the thickness of aECM corresponding to TEMs. Data were measured in 6 tracheal tubes of 3 adults for each treatment. ***P < 0.001 (Mann-Whitney nonparametric test). Data are represented as mean ± SEM. (**D**) Young's modulus of trachea treated 1% O_2 for 12h after ds*GFP* or ds*Muc91C* injection (N = 10 tracheal tubes for each treatment). *P < 0.05 (Mann-Whitney nonparametric test). The internal lines are medians, edges of the boxes are interquartile ranges and whiskers are ranges. (**E**) Number of residual PWN released from every 0.3g beetle incubated with PWN (N = 6 and 7 adults, respectively). ds*GFP* or ds*Muc91c* is injected before incubation. **P < 0.01 (Student's t-test, unpaired and two-tailed). Data are represented as mean ± SEM.

Discussion

Vector competence is important for vector-borne pathogens' transmission, but the

underlying mechanism remains largely unexplored. Here, we demonstrate one of strategies that PWN utilizes to maintain itself in its vector by modulating the vector beetle's hypoxia responses. This strategy helps the nematode to reach high numbers even in a single vector beetle and may consequently promote the successful spread, establishment and outbreak of pine wilt disease. Mechanically, we propose that PWN's loading process in vector beetles follows a positive feedback loop (**Figure 6**). First, continuous entering of nematodes into trachea decreases oxygen levels, resulting in hypoxia, which in turn increases the elasticity of tracheal tubes by upregulating *Muc91C*. The more elastic tube structure, in turn, allows more nematodes to reside in the lumen until maximum elasticity is reached, resulting in decreased gas transfer due to physical blocking caused by nematodes. Finally, the resulting high level of CO_2 drives nematodes away from the trachea (Wu et al., 2019). Thus, the nematodes strategically manage their loading and departure from the vector by manipulating oxygen supply in the vectors' trachea.

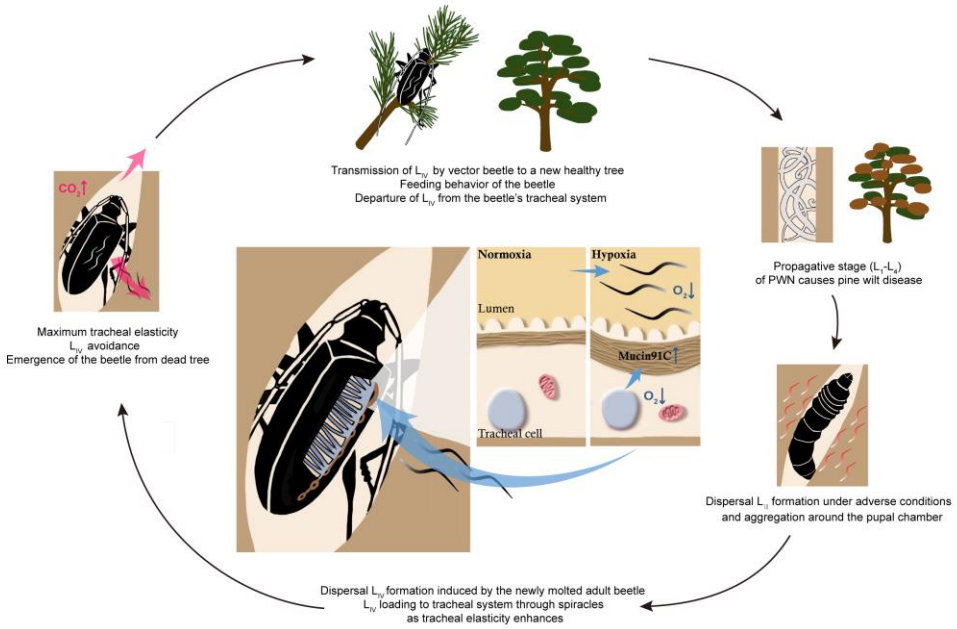

Figure 6. Schematic diagram of the feedback regulation of PWN loading through O_2 and CO_2 level in the tracheal system of *M. alternatus* When L_{IV} dispersal nematodes continuously enter the vector beetle through spiracles, the consequent hypoxia enhances the elasticity of tracheal tubes by upregulating *Muc91C*. The more elastic tube structure, in turn, allows more nematodes to reside in the lumen. When tracheal tubes reach to their maximum elasticity, nematodes influence gas exchange of beetles and the resultant high level of CO_2 drives nematodes away from the trachea.

Hypoxia occurs universally across living organisms and plays multiple roles in hosts infected by pathogens. For instance, a protozoan parasite *Leishmania donovani* induces inflammatory hypoxia to limit the capacity of the host's myeloid cells to kill the parasite (Hammami et al., 2017). Some commensal gut microbiota maintain epithelial hypoxia to limit the growth of enteric pathogens in the gut lumen of chicks (Litvak et al., 2019). However, hypoxia in pathogen-vector relationships has long been a neglected research topic. Our study shows that retention of nematodes caused hypoxia in tracheal tubes of vector beetles, providing empirical evidence for a previous hypothesis that the heavy PWN loading hinders the gas exchange of the beetle (Togashi and Sekizuka, 1982). Such hypoxia induced by PWN loading improved the vector's tracheal capacity to harbor PWN. The correlation between hypoxia and vector competence can be extrapolate to the interaction between circulative pathogens and their vectors, because their migration, replication or propagation processes inside vectors may also increase oxygen demands and result in hypoxia.

Mechanical properties of tracheal tube are critical to luminal volume by regulating

385 tubular size (Dong et al., 2014) and supporting tracheal deformation for air convection
386 (Westneat et al., 2003). Our results show that after heavy PWN loading or hypoxic
387 treatment, the elasticity of the tracheal tubes of the vector beetle are remarkably
388 enhanced, indicating changes in tracheal geometry and the capacity to deflate and
389 inflate to meet high oxygen demand. In the PWN-beetle system, heavy PWN loading
390 occupies luminal volume needed by tracheal ventilation for the beetle's regular
391 respiration or intensive respiration during dispersal flight in the search of suitable host
392 pine trees. The enhanced tracheal elasticity adapts vector insects to hypoxic stress
393 allowing more oxygen inhalation and provides adequate lumen volume to carry large
394 numbers of nematodes. Therefore, altered mechanical properties of the beetles' trachea
395 after PWN loading likely maintains a balance between a limited fitness cost to beetles
396 and high vector competence for effective transmission of PWN.

397 Although aECM is crucial to determine mechanical properties of tubular organs
398 including trachea, the role of its molecular components remains largely unknown.
399 Along with enhanced tracheal elasticity in the vector beetle, our study also found
400 remarkable global expression changes of aECM genes after PWN loading. Using gene
401 manipulation, we further identified *Muc91C,* which encodes a resilin-like protein in
402 aECM, as the key component responsible for the thickening of non-chitin aECM layer
403 and the improved tracheal elasticity. However, due to incomplete reduced elasticity
404 under hypoxic condition in ds*Muc91C*-injected beetles, other tracheal cellular
405 components such as proteins embedded in the membrane may also regulate tracheal
406 elasticity. Structurally, Muc91C in *M. alternatus* contains two types of repeat motifs

but lacks chitin-binding RR2, a consensus sequence in resilin monomers (pro-resilins)(Michels et al., 2016), suggesting that its elasticity trait resides in the repeat motifs. Consistent with the absence of pro-resilin in the tracheal tubes of vector beetles, *Drosophilia* larval foregut is devoid of pro-resilin, but contains resilin-like Cpr56F (Lerch et al., 2020). Collectively, these examples suggest that resilin-like proteins are employed instead of resilin monomers in deformation of various cuticle-free organs. Because mucins are highly glycosylated macromolecule proteins, protecting cells against microbial infection (Martens et al., 2018), higher *Muc91C* in trachea may also contribute to maintaining the integrity of mucosal barriers to alleviate the detrimental effects of nematodes invasion, such as increased ROS reported in previous studies (Zhou et al., 2018).

The present study found that hypoxia promotes tracheal elasticity by upregulating the expression of *Muc91C*, suggesting that *Muc91C* is related to hypoxia adaptation. Similarly, significant upregulated expression of pro-resilin has been demonstrated in an intertidal crustacean, the copepod *Tigriopus californicus*, when exposed to extremely low oxygen levels (Graham and Barreto, 2019). Therefore, the sensitivity of gene expression of aECM components in epithelial tissues to hypoxia is likely a pervasive phenomenon in arthropods. Clustering into a separate lineage in the Mucin phylogenetic tree (**Figure 4-figure supplement 1**), all insect Muc91C proteins investigated in this study had no human homologues and were only distantly related to other mucins, suggesting their independent evolutionary origin in insects. In Asian longhorned beetles (*Anoplophora glabripennis*), for instance, AgMuc91C has 84%

sequence similarity with *MaMuc91C* (**Figure 4**). Therefore, further examination of *Muc91C* expression patterns and its responses to hypoxia in other pine sawyer beetles closely related to our study species, such as *Monochamus saltuarius* can help to assess the role of *Muc91C* in facilitating heavy PWN loading and thus to pine wood disease. Overall, our study provides evidence of exploitation of hypoxia-enhanced tracheal elasticity by a plant parasitic nematode to improve vector competence in this unique pathogen-vector system and offers new insights for the development of novel targets to control the pine wilt disease.

Materials and methods

Collection and rearing of nematodes and beetles

Mature larvae of sawyer beetles (*M. alternatus*) were collected from dead pine trees in the Fuyang area, Hangzhou City, Zhejiang Province, and reared in an incubator (26°C, humidity 35%) until they pupated or for seven days after eclosion. *B.xylophilus* were originally acquired from infected trees in Shannxi Province and maintained with *Botrytis cinerea* in potato dextrose agar (BD, 213400) plates at 25°C for generations until used in the experiments.

Nematode loading, tracheal dissections, and nematode quantification

50ml Erlenmeyer flasks containing *B. cinerea* growing in autoclaved (121°C, 30min) barley medium (10g barley in 15ml water) for two weeks at 25°C, were inoculated with 1,000 propagative nematodes. After the nematodes had fed for five days, autoclaved

449 pine wood sawdust layer was spread on top of the barley layer of the rearing flasks and
450 cultured in 4°C for another two weeks. When the color of the pupae's eyes turned dark,
451 they were put on the nematode-infected sawdust layer until six days after eclosion.
452 Emerged adult beetles were dissected by ventral filleting, and the tracheal tubes located
453 on both sides of the thorax were dissected under a stereomicroscope (Olympus SZX16,
454 Japan). The excised tracheal tubes and the left part of the body were washed in PBST
455 (Solarbio, P1033) to irrigate the nematodes and presence of nematode was confirmed
456 under a stereomicroscope (Olympus SZX16, Japan). The total number of isolated
457 nematodes per beetle were counted in plates with an inverted microscope (Olympus
458 CKX41, Japan).

459 **Measurement of oxygen concentrations**

460 The measurement of oxygen concentrations followed previous studies with
461 modifications (Brune et al., 1995; Pettersen et al., 2005). The Oxygen Microsensors
462 with tip diameters of 25 μm (Unisense OX-25-905248, Denmark) and 100 μm
463 (Unisense OX-100-909667, Denmark), respectively, were used to penetrate into trachea
464 tubes (which are visible after ventral filleting and gut removal) and poke into the atrium
465 cavity of the largest spiracles located on both sides of the thorax. This protocol was
466 used for beetles without or with nematodes to obtain high-resolution profiles of oxygen
467 concentrations. Prior to use, the electrodes of the microsensors were polarized overnight
468 in deionized and continuously aerated water. Calibration was carried out before and
469 after each experiment and was done by measuring the current when the microelectrode

470 was placed in water saturated with air (21kPa O_2) and measuring the background
471 current in 1% Na_2SO_3 (0kPa O_2). The values were measured with an amperemeter
472 (Unisense oximeter-5591, Denmark) connected to a computer with a software
473 SensorTrace Logger (Unisense, Denmark). Oxygen microsensor was fixed on a
474 micromanipulator. Once placed into tracheal tubes and poking into the atrium cavity
475 under a stereomicroscope, the microsensor was paused for at least 20s to ensure
476 sufficient data collection. The microsensor was then pulled out and recording was
477 continued for 15s to record values of the ambient air. To take into account temperature
478 derived fluctuation in saturated oxygen concentration of different tests, we converted
479 the concentrations to its corresponding partial pressure, and the average partial pressure
480 of oxygen during the 20s inside the trachea was calculated as the final data.

481 **Hypoxic treatment**

482 Hypoxic treatment was performed in a hypoxic chamber (FLYDWC-50; Fenglei Co.,
483 Ltd, China) placed in an artificial box to automatically control the ambient temperature,
484 air flow and pressure of oxygen (PO_2). Adult beetles without nematodes were placed in
485 the ventilated chamber, in which air flow was balanced with pure nitrogen to achieve
486 the required 1% O_2. The adult beetles were maintained in the chamber for 6h, 12h, or
487 24h at 25 ± 1 °C in the dark.

488 **Measurement of mechanical properties with tensile testing**

489 The two longest tracheal tubes linking the largest spiracle on both sides of the thorax

490 and the spiracle basal to the head of the beetle were dissected as mentioned above and
491 were maintained at room temperature (RT) in PBS (Solarbio, P1020). According to a
492 previous study on muscle fibers (Kaiser et al., 2019), tensile testing was performed with
493 a micromechanical system (Aurora Scientific, Ontario, Canada) equipped with a length
494 controller (322C), a 10mN force transducer (405A), and dynamic control software suite
495 DMC (ASI 600A). The measurements were performed inside a bath with PBS at room
496 temperature. The dissected tracheal tubes were tied to the fixed hooks at the ends of
497 length controller and force transducer using nylon fibers. Prior to testing, the
498 unstretched lengths (L_0) and radius (r) of the tubes were measured with caliper under
499 an inverted microscope (Olympus CKX41, Japan). All samples were tested at a constant
500 strain rate of 10% L_0/ 3 sec until failure or 2 × L_0. The stiffness of the tubes was
501 characterized by the Young's modulus (E) determined from the linear region of the
502 stress-strain curve, usually between 30% and 80% strain, using the equation of $E = \{(F$
503 $/ \pi r^2) / (\Delta L/ L_0)\}$.

504 **Transmission electron microscopy of the tracheal tubes**

505 The two longest tracheal tubes linking the largest spiracle on both sides of the thorax
506 and the spiracle basal to head of the beetle were dissected and instantly fixed with 2.5%
507 (vol/vol) glutaraldehyde (Coolaber, SL1790) and 4% (vol/vol) paraformaldehyde
508 (Solarbio, P1112) with Phosphate Buffer (PB) (0.1 M, pH 7.4) (Macklin, H885798).
509 The samples were then washed four times in PB and then tubes were postfixed with 1%
510 (wt/vol) osmium tetraoxide in PB for 2 h at 4 °C, dehydrated through a graded ethanol

511 series (30, 50, 70, 80, 90, 100%, 100%, 7min each) into pure acetone (2×10min).
512 Samples were infiltrated in graded mixtures (3:1, 1:1, 1:3) of acetone and SPI-PON812
513 resin (16.2 g SPI-PON812, 10 g DDSA and 8.9 g NMA), and then changed to pure resin.
514 Finally, tubes were embedded in pure resin with 1.5% BDMA and polymerized for 12h
515 at 45°C, 48 h at 60°C. The ultrathin sections (70nm thick) were sectioned with
516 microtome (Leica EM UC6, Germany), double-stained by uranyl acetate and lead
517 citrate, and examined by a transmission electron microscope (FEI Tecnai Spirit120kV,
518 Oregon, USA).

519 **RNA-seq and Transcriptome analysis**

520 Each sample for RNA-seq was prepared by combining four individual beetles (two
521 females and two males, six days after emergence) for one library construction. The two
522 libraries included trachea of sawyer beetles with and without PWN. Tracheal tubes were
523 extirpated, washed with PBS to remove the nematodes, and immediately flash frozen
524 with Trizol (Invitrogen,15596018) and stored in -80°C before use. Total RNA was
525 isolated from the frozen samples using Trizol reagent according to the manufacturer's
526 protocol. mRNA was purified with a Dynabeads mRNA purification kit (Invitrogen,
527 61012). PolyA containing mRNAs was enriched with oligo (dT) magnetic beads (NEB,
528 S1419S), fragmented with RNA fragmentation reagent, and subjected to the following
529 procedure: first- and second-strand cDNA synthesis, purification, end repair, single-
530 nucleotide addition, ligation of adapters, purification of ligated products, and PCR
531 amplification for cDNA template enrichment. The RNA-seq library preparation kit for

532 whole transcriptome discovery (compatible with Illumina, San Diego, California, USA)
533 was used (Illumina Whole-Genome Gene Expression BeadChips). The 320 - 420bp
534 products were purified with the MiniElute gel extraction kit (Qiagen, Hilden, Germany)
535 and sequenced with the Illumina novaseq 6000 platform at Biomarker Technologies Co,
536 LTD.

537 **Identification and analysis of aECM-related genes from the transcriptome and**
538 **phylogenetic analysis**

539 Using the SignalP 3.0 (http://www.cbs.dtu.dk/services/SignalP), we predicted secreted
540 proteins in DEGs, based on the presence and extension of signal peptides. The retrieved
541 proteins were manually confirmed by Nr, GO, KO annotations, and using pfam and a
542 BlastX search against the amino acid sequences of known ECM-related genes from
543 flybase (http://flybase.org/). Transmembrane domains were analyzed by TMHMM
544 server v. 2.0 (http://www.cbs.dtu.dk/services/TMHMM/). The RR2 Consensus
545 sequences were predicted using the cuticleDB website
546 (http://bioinformatics2.biol.uoa.gr/cuticleDB/index.jsp). The O-glycosylation sites of
547 mucin proteins were determined by NetOGlyc 4.0
548 (www.cbs.dtu.dk/services/NetOGlyc). To verify the classification of resilin-related
549 proteins and other mucin proteins, phylogenetic analysis was performed using the full-
550 length amino acid sequences of representative proteins from other species retrieved
551 from the GenBank database. Multiple alignments of the amino acid sequences were
552 performed using the Clustal W program in MEGA 10.0. The phylogenetic trees were

553 constructed adopting neighbor-joining (NJ) method, using 1000 bootstrap repetitions.
554 All resilin-related and mucin sequences of other model species used in this study are
555 provided as **Figure 4-source data** and **Supplementary file 1**.

556 **Real-time PCR**

557 Total RNA was extracted from thoracic tracheal tubes of each beetle in different
558 treatments using TRIzol reagent according to the manufacturer's protocol and stored at
559 -80°C until used in experiments. The total number of nematodes in corresponding
560 tracheal samples were counted. RNA quality was assessed with an ND-1000
561 spectrophotometer (NanoDrop Technologies, Delaware, USA). About 1 μg of RNA was
562 used as template to produce cDNA with FastQuant RT kit with a genomic DNA eraser
563 (Tiangen, KR106). RT-qPCR was performed using Talent qPCR PreMix (SYBR Green)
564 (Tiangen, FP209) and on a 7300Plus Real-Time PCR system (Applied Biosystems,
565 Massachusetts, USA). At least five biological replicates were assayed for statistical
566 analysis. The amount of mRNA was calculated by the change in cycle threshold (ΔΔCt)
567 method and was normalized to control rp49 mRNA values. qPCR primers are listed in
568 **Supplementary file 2**.

569 **RNA interference**

570 Double-stranded RNAs (dsRNAs) were synthesized with cDNA templates possessing
571 T7 RNA polymerase promoter sequences on both ends (**Supplementary file 2**),
572 according to the T7 RiboMax Express RNAi System Kit (Promega, P1700) protocol.

573 Within two days after molting, approximately 60 adults beetle were injected at the joint
574 of the second and the third abdominal segment with 30 μg of dsRNA (< 5 μl) using a
575 7000-series modified microliter syringe (Hamilton, Bonaduz, Switzerland). Control
576 beetles were injected with dsGFP as a negative control. The injected adult beetles were
577 kept in standard conditions for four days, then treated with 1% O_2 for 12h. The injected
578 adult beetles used in the nematodes loading trial were kept in 50ml Erlenmeyer flasks
579 with barley medium containing dispersal L_{III} and L_{IV} nematodes at 25°C for 5 days. When
580 the adults were seven days old, they were dissected to obtain trachea samples for the
581 different assays, and disposed as described earlier.

582 **Statistical analysis**

583 The sample size is determined according to previous publications in the pine sawyer
584 beetle species (Wu et al., 2019; Zhao et al., 2016; Zhou et al., 2018). For nematode
585 loading, hypoxic treatments and RNAi treatments, individuals were randomly allocated
586 into experimental group and control group, and no restricted randomization was applied.
587 For nematode quantification, measurements of mechanical properties with tensile
588 testing, researchers were blind to RNAi or hypoxic treatments before counting or
589 measurements. All experiments were performed for at least 3 independent biological
590 replicates.
591 A Pearson correlation coefficient was used to measure the correlation between PWN
592 loading and partial pressure of oxygen. The semi-log fit using least square method was
593 chosen for curve fitting. The fit formula was $Y=10.55 + (-9.629) \times \log(X)$ with an R^2

value of 0.85. A Kolmogorov Smirnov test was used to check the normality of data. When the assumption of normal distribution was met, Student's t test and One-way ANOVA with Dunn's or Tukey's multiple comparison were used for two-group and three-group comparisons, respectively. When the assumption of normal distribution was not met, Mann-Whitney U test and Kruskal–Wallis with Dunn's multiple comparison were used for two-group and three-group comparisons, respectively. Statistical analysis was performed with Graphpad Prism 8.0 (Graphpad software, San Diego, California, USA).

Acknowledgements

This work was funded by the National Natural Science Foundation of China (32088102, 32061123002 and 31970466) and National Key Research and Development Program of China (2021YFC2600100). We are grateful to Yujia Xiang and Jin Ge for the assistance in bioinformatic analysis. We thank Kathryn E. Bushley for reviewing the manuscript.

Author contribution

X.T., J.Z., L.Z. and J.S. conceived and designed the experiments. J.S. supervised the study. X.T. performed loading and counting of PWN, tracheal dissection, tensile test. X.T and J.Z. conducted measurement of oxygen concentrations, TEM and transcriptomic analysis. X.T. and S.L. performed real-time PCR, RNA interference. S.L. provided the support for visualization of schematic diagram. X.T. prepared the

manuscript draft. X.T., J.Z., T. K. and J.S. revised the manuscript.

Additional files

Supplementary files:

Supplementary file 1. Species and GenBank accession no. of Pro-resilins and mucins.

Supplementary file 2. Primers for real-time qPCR and RNAi experiments.

Transparent reporting form

Data availability:

All data generated or analyzed during this study are included in the manuscript and supporting file; Source Data files have been provided for Figures 1, 2, 3, 4 and 5. The following dataset was generated:

Author(s)	Year	Dataset title	Dataset URL	Database and Identifier
Tang X	2022	RNA-seq of pine sawyer beetle with PWN	https://ngdc.cncb.ac.cn/gsa/s/98v9AiDE	bigd, CRA006464

References

Aikawa T. Transmission Biology of *Bursaphelenchus xylophilus* in Relation to Its Insect Vector[Book Section]. *Pine Wilt Disease*: 2008, 123-138.

Akbulut S, Stamps WT. Insect vectors of the pinewood nematode: a review of the biology and ecology of *Monochamus* species. *Forest Pathology*, 2012, **42**: 89-99. DOI:10.1111/j.1439-0329.2011.00733.x

Andersen SO. Studies on resilin-like gene products in insects. *Insect Biochemistry and Molecular Biology*, 2010, **40**: 541-551. DOI:10.1016/j.ibmb.2010.05.002

Bartholomay LC, Michel K. Mosquito Immunobiology: The Intersection of Vector Health and Vector Competence. *Annual Review of Entomology*, 2018, **63**: 145-167. DOI:10.1146/annurev-ento-010715-023530

Brune A, Emerson D, Breznak JA. The termite gut microflora as an oxygen sink: microelectrode determination of oxygen and pH gradients in guts of lower and higher termites. *Applied And*

638 *Environmental Microbiology*, 1995, **61**: 2681-2687.
639 Centanin L, Gorr TA, Wappner P. Tracheal remodelling in response to hypoxia. *Journal of Insect*
640 *Physiology*, 2010, **56**: 447-454. DOI:10.1016/j.jinsphys.2009.05.008
641 Chen AYS, Walker GP, Carter D, Ng JCK. A virus capsid component mediates virion retention and
642 transmission by its insect vector. *PNAS*, 2011, **108**: 16777-16782.
643 DOI:10.1073/pnas.1109384108
644 Chen Y, Chen Q, Li M, Mao Q, Chen H, Wu W, Jia D, Wei T. Autophagy pathway induced by a plant
645 virus facilitates viral spread and transmission by its insect vector. *PLoS Pathogens*, 2017, **13**:
646 e1006727. DOI:10.1371/journal.ppat.1006727
647 Coon KL, Valzania L, McKinney DA, Vogel KJ, Brown MR, Strand MR. Bacteria-mediated hypoxia
648 functions as a signal for mosquito development. *PNAS*, 2017, **114**: E5362-E5369.
649 DOI:10.1073/pnas.1702983114
650 Dai J, Estrada B, Jacobs S, Sanchez-Sanchez BJ, Tang J, Ma M, Magadan-Corpas P, Pastor-Pareja JC,
651 Martin-Bermudo MD. Dissection of Nidogen function in *Drosophila* reveals tissue-specific
652 mechanisms of basement membrane assembly. *PLoS Genetics*, 2018, **14**: e1007483.
653 DOI:10.1371/journal.pgen.1007483
654 Dong B, Hannezo E, Hayashi S. Balance between apical membrane growth and luminal matrix resistance
655 determines epithelial tubule shape. *Cell Reports*, 2014, **7**: 941-950.
656 DOI:10.1016/j.celrep.2014.03.066
657 Dong B, Hayashi S. Shaping of biological tubes by mechanical interaction of cell and extracellular matrix.
658 *Current Opinion in Genetics & Development*, 2015, **32**: 129-134.
659 DOI:10.1016/j.gde.2015.02.009
660 Eigenbrode SD, Bosque-Perez NA, Davis TS. Insect-borne plant pathogens and their vectors: ecology,
661 evolution, and complex interactions. *Annual Review of Entomology*, 2018, **63**: 169-191.
662 DOI:10.1146/annurev-ento-020117-043119
663 Fielding NJ, Evans HF. The pine wood nematode *Bursaphelenchus xylophilus* (Steiner and Buhrer)
664 Nickle (= *B. lignicolus* Mamiya and Kiyohara): an assessment of the current position. *Forestry*,
665 1996, **69**: 35-46.
666 Glasheen BM, Robbins RM, Piette C, Beitel GJ, Page-McCaw A. A matrix metalloproteinase mediates
667 airway remodeling in *Drosophila*. *Developmental Biology*, 2010, **344**: 772-783.
668 DOI:10.1016/j.ydbio.2010.05.504
669 Graham AM, Barreto FS. Loss of the HIF pathway in a widely distributed intertidal crustacean, the
670 copepod *Tigriopus californicus*. *PNAS*, 2019, **116**: 12913-12918.
671 DOI:10.1073/pnas.1819874116
672 Gray JS, Estrada-Pena A, Zintl A. Vectors of Babesiosis. *Annual Review of Entomology*, 2019, **64**: 149-
673 165. DOI:10.1146/annurev-ento-011118-111932
674 Greenlee KJ, Socha JJ, Eubanks HB, Pedersen P, Lee WK, Kirkton SD. Hypoxia-induced compression
675 in the tracheal system of the tobacco hornworm caterpillar, *Manduca sexta*. *Journal of*
676 *Experimental Biology*, 2013, **216**: 2293-2301. DOI:10.1242/jeb.082479
677 Hammami A, Abidin BM, Charpentier T, Fabie A, Duguay AP, Heinonen KM, Stager S. HIF-1α is a key
678 regulator in potentiating suppressor activity and limiting the microbicidal capacity of MDSC-
679 like cells during visceral leishmaniasis. *PLoS Pathogens*, 2017, **13**: e1006616.
680 DOI:10.1371/journal.ppat.1006616
681 Harrison JF, Greenlee KJ, Verberk WCEP. Functional hypoxia in insects: definition, assessment, and

consequences for physiology, ecology, and evolution. *Annual Review of Entomology*, 2018, **63**: 303-325. DOI:10.1146/annurev-ento-020117-043145

Hayashi S, Kondo T. Development and function of the *Drosophila* tracheal system. *Genetics*, 2018, **209**: 367-380. DOI:10.1534/genetics.117.300167

Huang HJ, Bao YY, Lao SH, Huang XH, Ye YZ, Wu JX, Xu HJ, Zhou XP, Zhang CX. Rice ragged stunt virus-induced apoptosis affects virus transmission from its insect vector, the brown planthopper to the rice plant. *Scientific Reports*, 2015, **5**: 11413. DOI:10.1038/srep11413

Jang S, Mergaert P, Ohbayashi T, Ishigami K, Shigenobu S, Itoh H, Kikuchi Y. Dual oxidase enables insect gut symbiosis by mediating respiratory network formation. *PNAS*, 2021, **118**: e2020922118. DOI:10.1073/pnas.2020922118

Kaiser NJ, Kant RJ, Minor AJ, Coulombe KLK. Optimizing blended collagen-fibrin hydrogels for cardiac tissue engineering with human iPSC-derived cardiomyocytes. *ACS Biomaterials Science and Engineering*, 2019, **5**: 887-899. DOI:10.1021/acsbiomaterials.8b01112

Kusuma S, Zhao S, Gerecht S. The extracellular matrix is a novel attribute of endothelial progenitors and of hypoxic mature endothelial cells. *FASEB Journal*, 2012, **26**: 4925-4936. DOI:10.1096/fj.12-209296

Lataillade LG, Vazeille M, Obadia T, Madec Y, Mousson L, Kamgang B, Chen CH, Failloux AB, Yen PS. Risk of yellow fever virus transmission in the Asia-Pacific region. *Nature Communications*, 2020, **11**: 5801. DOI:10.1038/s41467-020-19625-9

Lerch S, Zuber R, Gehring N, Wang Y, Eckel B, Klass KD, Lehmann FO, Moussian B. Resilin matrix distribution, variability and function in *Drosophila*. *BMC Biology*, 2020, **18**: 195. DOI:10.1186/s12915-020-00902-4

Litvak Y, Mon KKZ, Nguyen H, Chanthavixay G, Liou M, Velazquez EM, Kutter L, Alcantara MA, Byndloss MX, Tiffany CR, Walker GT, Faber F, Zhu Y, Bronner DN, Byndloss AJ, Tsolis RM, Zhou H, Baumler AJ. Commensal *Enterobacteriaceae* protect against *Salmonella* colonization through oxygen competition. *Cell Host & Microbe*, 2019, **25**: 128-139.e125. DOI:10.1016/j.chom.2018.12.003

Llimargas M, Strigini M, Katidou M, Karagogeos D, Casanova J. Lachesin is a component of a septate junction-based mechanism that controls tube size and epithelial integrity in the *Drosophila* tracheal system. *Development*, 2004, **131**: 181-190. DOI:10.1242/dev.00917

Luschnig S, Bätz T, Armbruster K, Krasnow MA. *Serpentine* and *vermiform* encode matrix proteins with chitin binding and deacetylation domains that limit tracheal tube length in *Drosophila*. *Current Biology*, 2006, **16**: 186-194. DOI:10.1016/j.cub.2005.11.072

Martens EC, Neumann M, Desai MS. Interactions of commensal and pathogenic microorganisms with the intestinal mucosal barrier. *Nature Reviews Microbiology*, 2018, **16**: 457-470. DOI:10.1038/s41579-018-0036-x

McGettrick AF, Corcoran SE, Barry PJ, McFarland J, Cres C, Curtis AM, Franklin E, Corr SC, Mok KH, Cummins EP, Taylor CT, O'Neill LA, Nolan DP. *Trypanosoma brucei* metabolite indolepyruvate decreases HIF-1alpha and glycolysis in macrophages as a mechanism of innate immune evasion. *PNAS*, 2016, **113**: E7778-E7787. DOI:10.1073/pnas.1608221113

Michels J, Appel E, Gorb SN. Functional diversity of resilin in Arthropoda. *Beilstein Journal of Nanotechnology*, 2016, **7**: 1241-1259. DOI:10.3762/bjnano.7.115

O'Neill K, Olson BJ, Huang N, Unis D, Clem RJ. Rapid selection against arbovirus-induced apoptosis during infection of a mosquito vector. *PNAS*, 2015, **112**: E1152-E1161.

DOI:10.1073/pnas.1424469112
Öztürk-Çolak A, Moussian B, Araújo SJ. *Drosophila* chitinous aECM and its cellular interactions during tracheal development. *Developmental Dynamics*, 2016, **245**: 259-267. DOI:10.1002/dvdy
Pettersen EO, Larsen LH, Ramsing NB, Ebbesen P. Pericellular oxygen depletion during ordinary tissue culturing, measured with oxygen microsensors. *Cell Proliferation*, 2005, **38**: 257-267.
Togashi K, Sekizuka H. Influence of the pine wood nematode, *Bursaphelenchus lignicolus* (Nematoda: Aphelenchoididae), on longevity of its vector, *Monochamus alternatus* (Coleoptera: Cerambycidae). *Applied Entomology and Zoology*, 1982, **17**: 160-165.
Togashi K. Transmission Curves of *Bursaphelenchus xylophilus* (Nematoda: Aphelenchoididae) from Its Vector, *Monochamus alternatus* (Coleoptera: Cerambycidae), to Pine Trees with Reference to Population Performance. *Applied Entomology and Zoology*, 1985, **20**: 246-251.
Uzest M, Gargani D, Drucker M, Hébrard E, Garzo E, Candresse T, Fereres A, Blanc S. A protein key to plant virus transmission at the tip of the insect vector stylet. *PNAS*, 2007, **104**: 17959-17964.
Valzania L, Coon KL, Vogel KJ, Brown MR, Strand MR. Hypoxia-induced transcription factor signaling is essential for larval growth of the mosquito *Aedes aegypti*. *PNAS*, 2018, **115**: 457-465. DOI:10.1073/pnas.1719063115
Webster MR, De Vita R, Twigg JN, Socha JJ. Mechanical properties of tracheal tubes in the American cockroach (*Periplaneta americana*). *Smart Materials and Structures*, 2011, **20**: 094017. DOI:10.1088/0964-1726/20/9/094017
Wei J, He YZ, Guo Q, Guo T, Liu YQ, Zhou XP, Liu SS, Wang XW. Vector development and vitellogenin determine the transovarial transmission of begomoviruses. *PNAS*, 2017, **114**: 6746-6751. DOI:10.1073/pnas.1701720114
Westneat MW, Betz O, Blob RW, Fezzaa K, Cooper WJ, Lee WK. Tracheal respiration in insects visualized with synchrotron x-ray imaging. *Science*, 2003, **299**: 558-560. DOI:doi:10.1126/science.1078008
Wilkin MB, Becker MN, Mulvey D, Phan I, Chao A, Cooper K, Chung HJ, Campbell ID, Baron M, MacIntyre R. *Drosophila* Dumpy is a gigantic extracellular protein required to maintain tension at epidermal–cuticle attachment sites. *Current Biology*, 2000, **10**: 559-567.
Wu Y, Wickham JD, Zhao L, Sun J. CO_2 drives the pine wood nematode off its insect vector. *Current Biology*, 2019, **29**: R619-R620. DOI:10.1016/j.cub.2019.05.033
Zeitouni NE, Chotikatum S, von Kockritz-Blickwede M, Naim HY. The impact of hypoxia on intestinal epithelial cell functions: consequences for invasion by bacterial pathogens. *Molecular and Cellular Pediatrics*, 2016, **3**: 14. DOI:10.1186/s40348-016-0041-y
Zhao L, Mota M, Vieira P, Butcher RA, Sun J. Interspecific communication between pinewood nematode, its insect vector, and associated microbes. *Trends in Parasitology*, 2014, **30**: 299-308. DOI:10.1016/j.pt.2014.04.007
Zhao L, Zhang X, Wei Y, Zhou J, Zhang W, Qin P, Chinta S, Kong X, Liu Y, Yu H, Hu S, Zou Z, Butcher RA, Sun J. Ascarosides coordinate the dispersal of a plant-parasitic nematode with the metamorphosis of its vector beetle. *Nature Communications*, 2016, **7**: 12341. DOI:10.1038/ncomms12341
Zhao X, Zhang J, Yang J, Niu N, Zhang J, Yang Q. Mucin family genes are essential for the growth and development of the migratory locust, *Locusta migratoria*. *Insect Biochemistry and Molecular Biology*, 2020, **123**: 103404. DOI:10.1016/j.ibmb.2020.103404
Zhou J, Zhao LL, Yu HY, Wang YH, Zhang W, Hu SN, Zou Z, Sun JH. Immune tolerance of vector beetle

to its partner plant parasitic nematode modulated by its insect parasitic nematode. *FASEB Journal*, 2018, **32**: 4862-4877. DOI:10.1096/fj.201800247R

Zuo L, Iordanou E, Chandran RR, Jiang L. Novel mechanisms of tube-size regulation revealed by the *Drosophila* trachea. *Cell and Tissue Research*, 2013, **354**: 343-354. DOI:10.1007/s00441-013-1673-z

Figure supplements

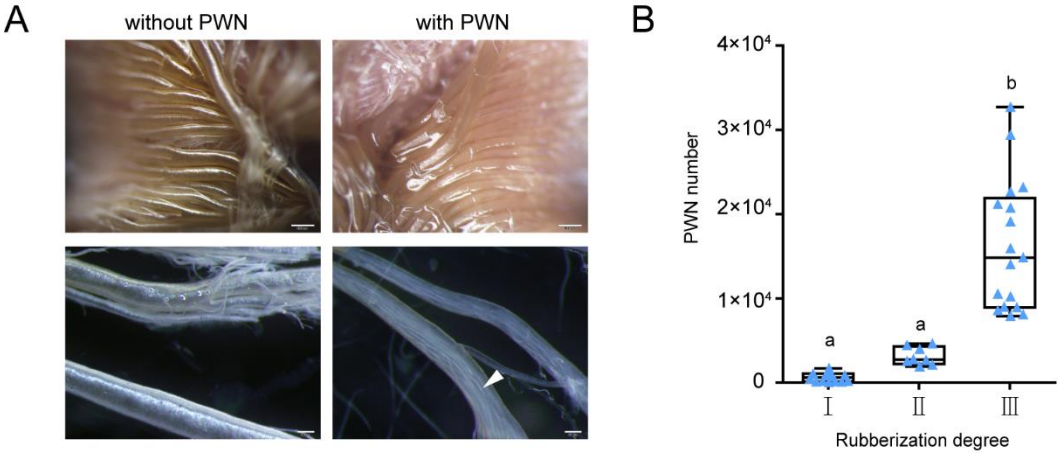

Figure 2-figure supplement 1. Morphological changes of trachea of *M. alternatus* after PWN loading. (**A**) Morphology of thoracic tracheal tubes without and with heavy PWN under stereoscopic microscope. Images in the upper (scale bar = 500μm) or lower (scale bar = 50μm) panel show trachea in vivo and in PBS solution, respectively. White arrow pinpoints PWN inside trachea tubes. Experiments were performed at least three times. (**B**) The relationship between total number of PWN per *M. alternatus* and degree of rubberization. According to the proportion of rubber-like tubes in all thoracic tracheal tubes, we sorted the trachea of beetles with PWN into three rubberization degrees (I, none; II, less than 50% rubber-like tubes; III, 50%~100% rubber-like tubes), and counted the number of PWN released from trachea. 39 adults, $N_I = 14$, $N_{II} = 8$, $N_{III} = 17$. Labels with different letters are significantly different at $P < 0.0001$ (Kruskal-Wallis test, followed by Dunn's multiple comparison test).

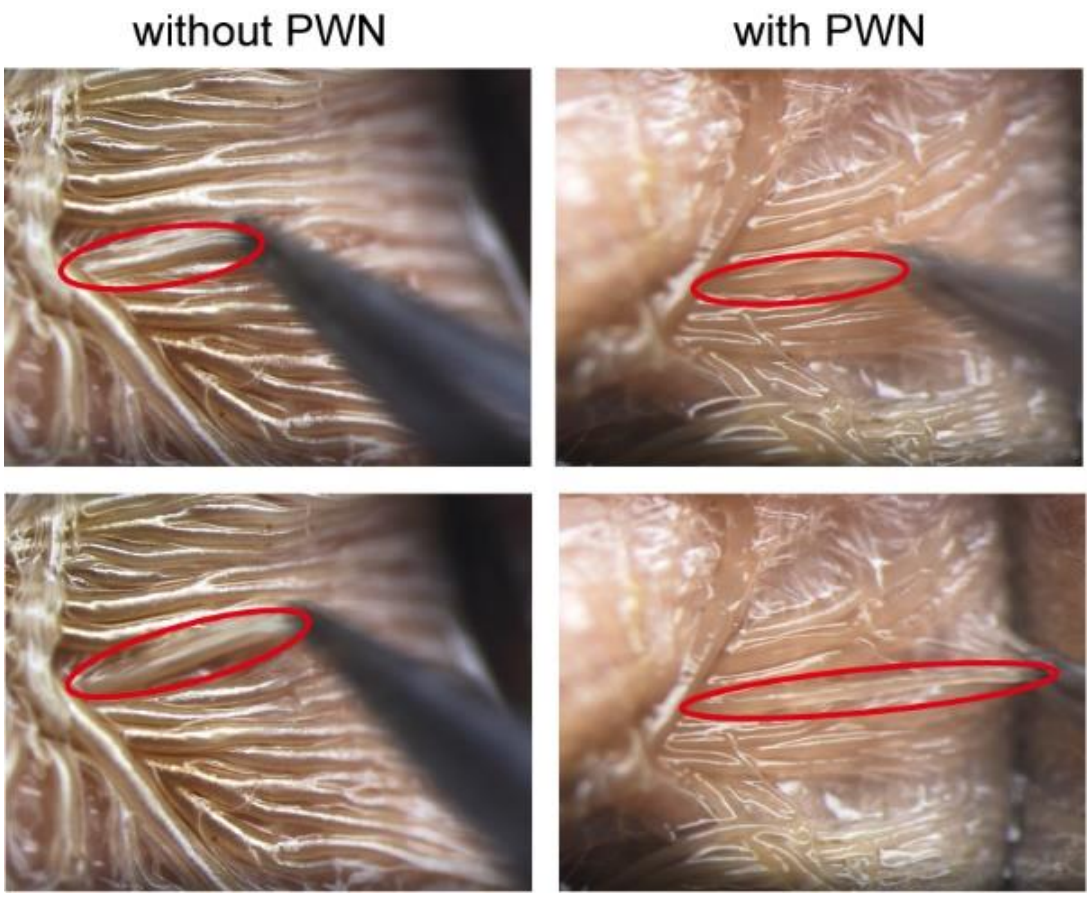

Figure 2-figure supplement 2. Pulling test of trachea of *M. alternatus* after PWN loading. Snapshots from videos imaged under stereotype microscope showed the pulling result of thoracic tracheal tubes with or without PWN. Red circles show one representative tubes in two groups before and after pulling.

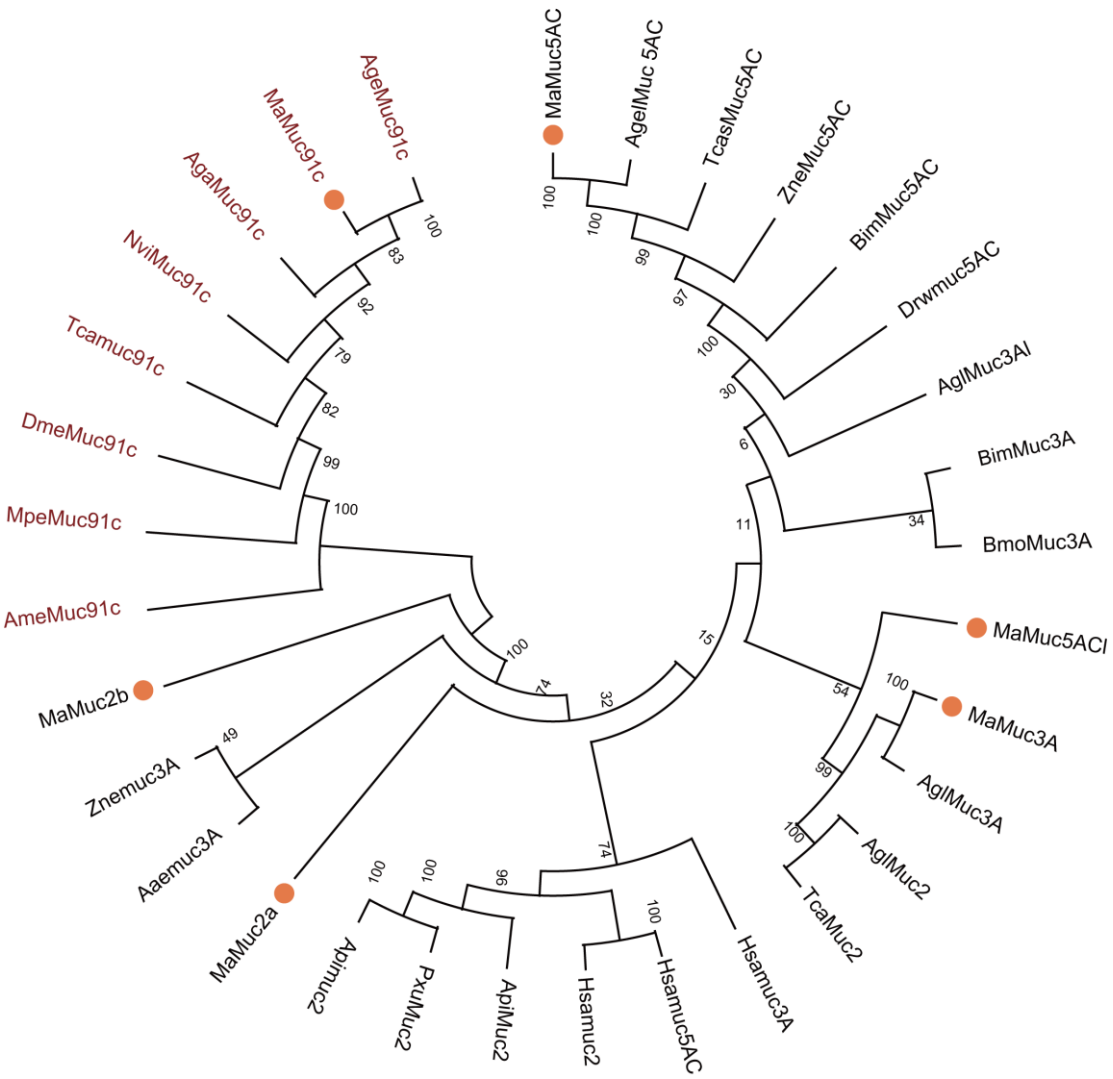

Figure 4-figure supplement 1. A phylogenetic tree constructed using *M. alternatus*. mucin sequences (orange dots) and other species' mucin sequences. Muc91C proteins were highlighted in red font. The full-length amino acid sequences of representative proteins were retrieved from the GenBank database. The phylogenetic tree was constructed with the MEGA 10.0 software based on a multiple alignment of the amino acid sequences performed by Clustal W, and adopting the NJ method. A bootstrap analysis of 1000 replications were used and 50% cut-off bootstrap values were applied to condense the tree. The sequence numbers of mucin or mucin-like proteins are listed in **Supplementary file 1**.

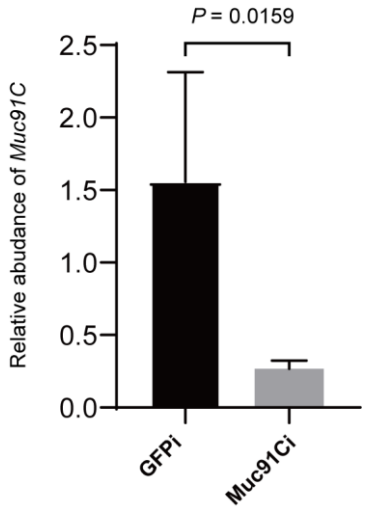

806

807 **Figure 5-figure supplement 1. RNAi efficiency of the Muc91C gene in adult beetles.**

808 Data are presented as mean ± SEM. N = 5. *P* value is determined by Mann-Whitney U

809 test.